Acta Cryst. (1968). A24, 240

Combined Laue- and Bragg-case X-ray Interferometers

BY U. BONSE
Physikalisches Institut, University of Münster, Germany
AND M. HART
H. H. Wills Physics Laboratory, University of Bristol, England

(*Received* 9 *June* 1967)

X-ray interference fringes are obtained with a new type of X-ray interferometer which utilizes both transmission and surface Bragg reflexion components. Unlike previous X-ray interferometers, the new system is *not* achromatic. Particular attention is paid to the geometric problems of preparation and to the problems imposed by the deviations from Bragg's Law which are caused by X-ray refraction. That the necessary geometric precision can be attained in practice is demonstrated by the observation of X-ray interference fringes when a lucite wedge is placed in one of the beam paths.

Introduction

Recently the construction and successful operation of X-ray interferometers was reported (Bonse & Hart, 1965*a*, *b*, *c*, 1966*a*, *b*). In those instruments the coherent beam splitting and beam recombination was accomplished either by the use of Laue-case diffraction, in which the diffracted wave leaves the crystal through the face opposite to the entrance surface, or by Bragg-case diffraction when the diffracted wave originates in the entrance surface of the crystal. Fig. 1 shows the arrangement of diffracting elements and of interfering beams that are generated in different parts of the single-crystal blocks from which the interferometers are cut. In each interferometer all the diffraction events are of the same type, *viz.* all are Bragg-case or all are Laue-case and all utilize the same set of Bragg planes. Since the coherence conditions and the overlap of interfering beams do not depend on the wavelength used, satisfactory operating conditions can be realised without strictly monochromatic radiation.

It is important that none of these interferometers embodies both Laue-case and Bragg-case diffracting components. Because the Bragg equation applies to diffracted waves inside a crystal, refraction at the crystal surfaces must be considered. The effect of refraction is to modify the Bragg equation so that, in the symmetric Bragg case with zero absorption (diffracting planes parallel to the crystal surface) one obtains (Darwin, 1914; Ewald, 1917)

$$2d \sin \theta_B = \lambda(1 + \delta \operatorname{cosec}^2\theta) \qquad (1)$$

while in the symmetric Laue case (diffracting planes normal to the crystal surface) we have

$$2d \sin \theta_L = \lambda \qquad (2)$$

where d is the spacing of the Bragg planes, λ is the X-ray wavelength and $(1-\delta)$ is the X-ray refractive index. θ_B, θ_L is the angle between the deviated diffracted beam and the Bragg planes at the centre of the reflexion range. Furthermore, under conditions when anomalous transmission is important, the peaks of the forward diffracted (T_L) beam and of the deviated diffracted (R_L) beam occur for different angles of incidence. The angular separation of the R_L and T_L peaks tends to zero when the normal absorption becomes very large. As a particular example Fig. 2 shows the angular variation of diffracted intensity in the symmetric Laue-case and in the symmetric Bragg case for the silicon 220 Bragg reflexion of copper $K\alpha$ radiation. When one requires consecutive Laue- and Bragg case diffraction in one crystal block the resultant diffracted intensity is low because $\theta_B \neq \theta_L(1,2)$. Large gains of intensity can be obtained if the diffracting crystals are tuned to one another by proper adjustment of either the angles of incidence or of the relative lattice parameters. Such tuning could be achieved by elastically

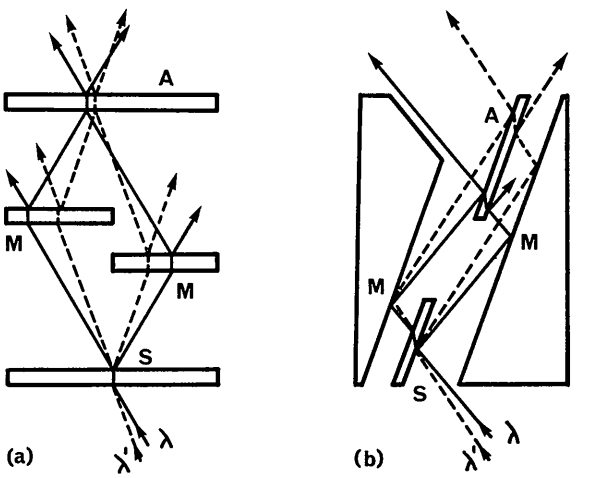

Fig. 1. Plan views of (*a*) Laue-case interferometer and (*b*) a Bragg-case interferometer. Each of the diffracting elements is part of a single-crystal block. *S* beam splitter, *M* mirrors, *A* analyser crystal. Geometrical overlap of coherent beams occurs separately for wavelengths λ and λ'.

deforming parts of the crystal block (Okkerse, 1963), so that the angle between the reflecting planes in the Bragg and Laue parts is $(\theta_B - \theta_L)$. Alternatively one can, for example, heat the Bragg-case parts so that the Bragg angle of the hotter crystals is equal to the Laue angle of the cooler. For the silicon 220 reflexion a temperature difference of approximately 17 °C is necessary. Experiments on mixed Laue–Bragg type interferometers which were tuned by heating the Bragg-case parts have been performed and will be described elsewhere.

This paper will show that interferometers using both Laue-and Bragg-case reflexions can be used without tuning. As with the Laue-case interferometers and the Bragg-case interferometer, the different components (beam splitter *S*, mirrors *M etc.*) are all connected parts of one monolithic crystal block.

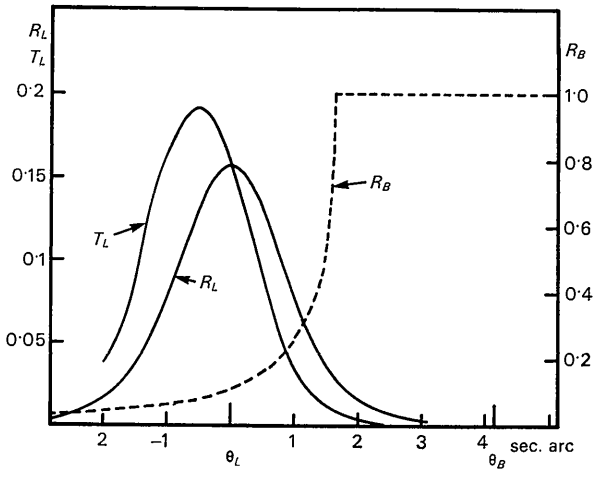

Fig. 2. Laue-case and Bragg-case reflexion intensities as a function of incident angle. R_B calculated in the zero absorption approximation. R_L, T_L calculated for a crystal thickness of 0·55 mm. Silicon 220 reflexion of copper $K\alpha$ radiation.

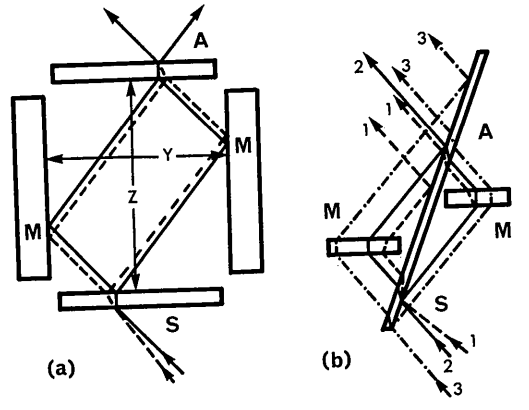

Fig. 3. Plans of two interferometers utilising both Bragg- and Laue-case diffraction. Ray paths for two different angles of incidence are shown by full and dashed lines. Each component is part of a single-crystal block with (*S*) beam splitter, (*M*) mirrors, (*A*) analyser. (*a*) L–B–L type (*b*) B–L–B type.

L-B-L and B-L-B interferometers

We will consider only the two interferometers in which both interfering beams have similar paths (Fig. 3). As before, the same set of Bragg planes is utilized for all the diffraction events in an interferometer. Each type can be specified by the sequence of diffraction occurring in one beam path so that the first, which has a Laue-case beam splitter, Bragg-case mirrors and Laue-case analyser [Fig. 3(*a*)] is called an L–B–L interferometer. Similarly, Fig. 3(*b*) shows a B–L–B interferometer in which the beam splitting and recombination is achieved in a very thin lamella cut at an angle to the Bragg planes so that a strong Bragg-case transmitted beam is produced.

For several reasons the L–B–L arrangement is much more satisfactory than the B–L–B arrangement. Since Bragg-case transmission is less efficient than Laue-case transmission in the range of wafer thicknesses available to us and since Laue-case mirrors involve an intensity loss of at least 50%, higher intensities can be expected with L–B–L interferometers than with B–L–B interferometers. With conventional diamond impregnated saws, widely used by the semi-conductor industry, the L–B–L type is easier to prepare than the B–L–B type.

Geometrical overlap of coherent beams

As shown earlier (Bonse & Hart, 1965*c*) coherent beams emerging from a region, which is typically a few microns wide*, on the entrance surface of an interferometer must finally overlap where the detector (photographic plate or counter) is located. Although this rather stringent condition is somewhat eased by the spread occurring within the various Borrmann triangles†, it means in practice that beams originating at one point in the beam splitter have to be brought together again on the analyser to within 5 to 50 μm. However, in contrast to the situation with Laue-case interferometers and Bragg-case interferometers, the necessary geometric conditions for the L–B–L and B–L–B interferometers are wavelength dependent. For example, beam overlap in the L–B–L case [Fig. 3(*a*)] occurs only when

$$\tan \theta_L = Y/Z \qquad (3)$$

where Y is the width and Z the length of the instrument. Equation (2) must also be satisfied, of course, so that monochromatic radiation is necessary.

Under normal conditions the incident radiation is sufficiently divergent to excite the full Borrmann fan of energy flow inside the crystal. One must therefore regard the incident beam as a coherent spherical wave rather than a simple plane wave and maintain geometrical overlap for all directions of incidence. This

* The effective size of the source is reduced to a few microns by the narrow angular acceptance of the crystal.

† This spread can be of order 100 μm and is very helpful, if not essential, for meeting the various geometric requirements in the manufacture of interferometers.

is straightforward in the L–B–L interferometer because the interfering waves always travel together as a wave-field in the beam splitter S and in the analyser A. However, in the B–L–B interferometer each wave travels separately through a Bragg-case transmission and a Laue-case transmission wafer. As the angular dispersion of energy flow inside the crystals is different in the two cases there is inevitably a deviation from ideal geometrical overlap of the two interfering rays as sketched in Fig. 3(*b*). The overlap is exact for rays of type 2 but rays of type 1, incident at a different angle but still within the range of reflexion of the interferometer lamellae, are no longer superimposed at the analyser. At best the mismatch will cause a reduction in fringe contrast.

Field of view

For useful interferometry the coherence conditions should be satisfied over a wide field of view. In a geometrically ideal L–B–L interferometer, pairs of coherent beams originating at a point on the exit surface of the beam splitter S overlap precisely at a conjugate point on the entrance surface of the analyser A. The field of view is therefore limited only by the size of available crystals.

With the B–L–B geometry of Fig. 3(*b*) the useful field is rather restricted. Although the overlap is exact for the beams originating from the incident beam 2, the two beams produced by the parallel but displaced beam 3 are spatially separated at the analyser and cannot interfere. This is a direct consequence of the obliquity of the Bragg-case lamellae but the situation could be improved, at the expense of intensity, by using instead a *symmetric Bragg-case transmission* beam splitter and analyser.

It seems for these reasons that B–L–B interferometers have few, if any advantages over the L–B–L type. They will not be considered further in the discussion.

Asymmetry of reflexion

Geometrically ideal interferometers cannot of course be realized in practice and it is pertinent to estimate the geometrical imperfection which is tolerable. Let us first consider the effect of errors in the orientation of the crystal surfaces. Fig. 4 shows the paths of a pair of coherent beams in an interferometer in which the surfaces of S and A are exactly normal to the Bragg planes but in which the mirrors M make small angles φ_l, φ_r with the Bragg planes. In other respects we assume that the interferometer is ideal. The origin O of a set of Cartesian coordinates is at the centre of the exit surface of the beam splitter S as shown and the ideal geometric situation is indicated by broken lines. From Fig. 4 it follows straightforwardly that the overlap error Δy on the analyser A is

$$\Delta y = \Delta y_l - \Delta y_r = 2y_0 \cot\theta[\varphi_l + \varphi_r] . \qquad (4)$$

For the silicon 220 reflexion with copper $K\alpha$ radiation and an orientation error $\varphi_l = \varphi_r = 0{\cdot}01°$ we find, for a field width $y_0 = 5$ mm, $\Delta y \simeq 8\ \mu$m. This is already approaching the maximum tolerable 'focusing' or overlap error. Furthermore, a precision of $0{\cdot}01°$ in the orientation of cut and chemically polished crystal surfaces is not easily attained.

Small rotations φ of the surfaces of the beam splitter S about an axis through O and normal to the yz plane introduces a focusing error

$$\Delta y = 2y_0\varphi \tan\theta \qquad (5)$$

again, with $\varphi = 0{\cdot}01°$, $y_0 = 5$ mm and for the silicon 220 reflexion of copper $K\alpha$ radiation, $\Delta y \simeq 0{\cdot}7\ \mu$m. This is therefore far less important than the effect of mirror asymmetry.

L-B-B-L interferometer

The focusing error caused by mirror asymmetry can be effectively eliminated by using the double Bragg-case mirror arrangement shown in Figs. 5 and 6. It is obvious that the defocusing effects in the lower and upper halves of the interferometer (Fig. 5) cancel to first order. For $\varphi_r, \varphi_l \ll \tan\theta$ the beam shifts on the analyser are

path I,	first Bragg reflexion	$+2\varphi_l(Y-y_0)\cot\theta$
path II,	first Bragg reflexion	$+2\varphi_r(Y+y_0)\cot\theta$
path I,	second Bragg reflexion	$+2\varphi_r[(Y+y_0)\cot\theta$
		$+2\varphi_l(Y-y_0)\cot^2\theta]$
path II,	second Bragg reflexion	$+2\varphi_l[(Y-y_0)\cot\theta$
		$-2\varphi_r(Y+y_0)\cot^2\theta]$,

so that the relative shift between the two beams is

$$\Delta y = 8\varphi_l\varphi_r Y \cot^2\theta . \qquad (6)$$

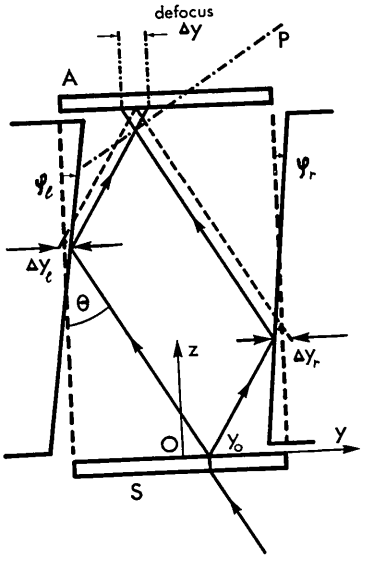

Fig. 4. The overlap error Δy in the L–B–L interferometer resulting from mirror orientation errors φ_l, φ_r. Dashed lines show the ideal geometric arrangement and full lines show beam paths when the mirror surfaces make angles φ_l, φ_r with the Bragg planes. Overlap points lie on the oblique plane P.

Since Δy is independent of y_0, all points of overlap lie in the plane P which is parallel to the plane of the analyser and separated from it by the distance ΔZ where

$$\Delta Z = \tfrac{1}{2}\varphi_l \varphi_r Y (2 \cot \theta)^3 \, . \quad (7)$$

If the length of the interferometer is carefully adjusted all of the overlap points can be made to coincide with the entrance surface of the analyser. Thus, small errors in the surface orientation of the Bragg-case mirrors can be compensated by slight modifications of the length to width ratio of the interferometer. For exam-

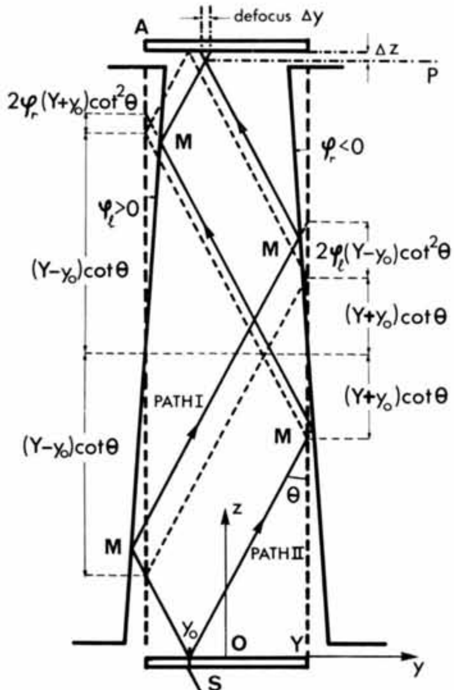

Fig. 5. As Fig. 4, L–B–B–L interferometer. Overlap points lie on the plane P which is parallel to the analyser crystal surface.

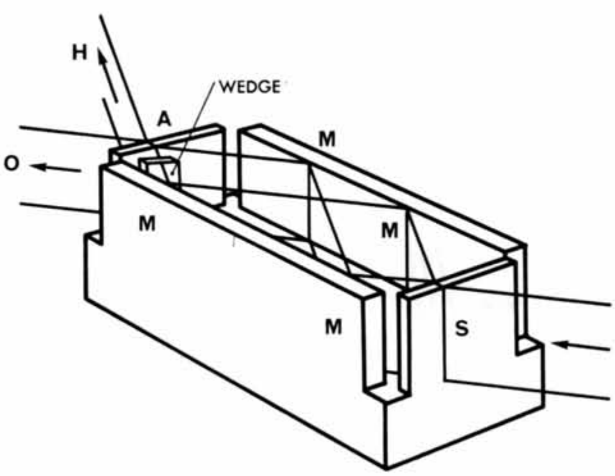

Fig. 6. Layout of the L–B–B–L interferometer. O exit beam parallel to the incident beam. H exit beam in the direction of diffracted beams. S beam splitter, M Bragg-case mirrors, A analyser. Interferograms were obtained with a lucite wedge in the position shown.

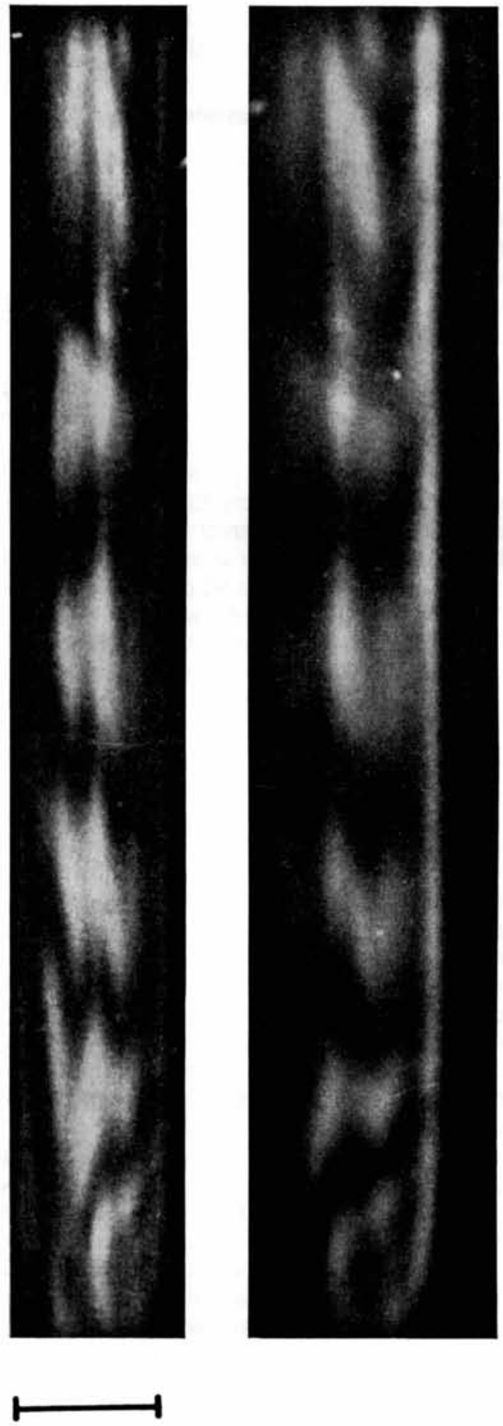

Fig. 7. Photograph of the exit beams obtained with the arrangement shown in Fig. 6. The plate was normal to the H-beam (left) so that the O-beam (right) is widened by oblique incidence. Note the horizontal interference fringes. Vertical stripes are caused by variations in the lattice parameter, see text. Scale mark 0·5 mm.

ple, with a silicon interferometer using the 220 reflexion of copper $K\alpha$ radiation $\Delta Z = 36\ \mu m$ for $\varphi_r = \varphi_l = 0{\cdot}5°$ and $Y = 1$ cm. Such corrections can be easily made by selective chemical polishing.

It follows that in practical L–B–B–L interferometers the useful field need be limited only by the size of available crystals.

Experiments

L–B–B–L interferometers were cut from dislocation free Lopex silicon crystals*. They were designed for copper $K\alpha_1$ radiation using the 220 reflexion, for which the length to width ratio ($2 \cot \theta$) is 4·567. The layout of wafers and mirrors is shown in Fig. 6. In all cases the surfaces were within 0·1″ of the ideal orientation so that the necessary length correction of $\Delta Z \leq 0{\cdot}72\ \mu m$ (equation (6), $Y = 5$ mm) is negligibly small. After all surfaces had been cut with a diamond-impregnated saw the material between the Bragg-case mirrors was removed by ultrasonic machining. Finally the interferometer was chemically polished† to remove the damaged surface layers of crystal. Chemical polishing was continued until the correct length to width ratio had been obtained – if the chemical polish removes material uniformly over the whole surface the actual length to width ratio decreases with polishing time.

Photographs of the O and H exit beams (Fig. 6) behind the analyser were taken on Ilford nuclear plates type L4. A Hilger microfocus X-ray source was used in these experiments to achieve good angular and spatial resolution with adequate intensity. At 40 kV and 3 mA, exposure times varied between 40 hr and 80 hr.

With a lucite wedge in one of the beams, as shown in Fig. 6, X-ray interference fringes were obtained in both the O and H beams, running parallel to the edge of the wedge (Fig. 7). The fringes disappear if either of the beams is removed by a lead stop. The measured fringe spacing is the same as that calculated from the known wedge angle and the refractive index of lucite. These topographs demonstrate clearly that mixed Laue–Bragg interferometers will perform satisfactorily even without tuning; with correct tuning and a high power X-ray source exposure times would be redued a thousandfold.

Close inspection of Fig. 7 shows that, although the X-ray interference fringes are the same in both beams, there are also very fine vertical stripes which are different in the two patterns. Similar effects have been observed before in Bragg-case interferometers (Bonse & Hart, 1966*b*). They do not disappear when one of the interfering beams is removed by a stop and they are thought to be the multiple reflexion topographic images of layered variations in lattice parameter caused by temperature fluctuations during crystal growth. Since the long axis of the interferometer is parallel to the growth axis of the original crystal the observed orientation of the stripes supports that hypothesis.

Closer inspection of the O-beam interferogram reveals that the interference fringe contrast is not constant across the field width, *i.e.* the contrast depends on the exact angle of incidence. In particular, the bright line on the right hand edge (which contributes strongly to the integrated reflexion) has little or no fringe contrast. Also, the contrast in the H-beam interferogram is generally better than that in the O-beam picture. These effects can be simply understood if we examine the relative intensities of interfering beams in more detail. In total there are four exit beams, two in the O direction and two in the H direction, one of each type from each beam path. The reflexion and transmission intensity factors associated with the beams are

$$\begin{aligned} O\text{-beams: path II } & R_L R_B R_B R_L = R_L^2 R_B^2 \\ \text{path I } & T_L R_B R_B T_L = T_L^2 R_B^2 \\ H\text{-beams: path II } & R_L R_B R_B T_L = R_L T_L R_B^2 \\ \text{path I } & T_L R_B R_B R_L = R_L T_L R_B^2 \ . \end{aligned}$$

These factors $T_L^2 R_B^2$, $R_L^2 R_B^2$ and $T_L R_L R_B^2$ vary considerably over the range of reflexion (Fig. 8). $T_L^2 R_B^2$ and $R_L^2 R_L^2$, the beams which overlap in the O-beam interferogram, do so with considerable amplitude differences, thus accounting for the lower contrast in the O-beam picture. We see that the bright line previously mentioned is part of the $R_L^2 R_B^2$ beam and that it could be eliminated if the width of the Laue-case reflexion curve were reduced by increasing the crystal thickness. However, in the H-beam the two interfering beams have the same intensity variation with angle of incidence. In the absence of geometric imperfections, the H-beam interferogram is therefore formed by exact superposition of two equal amplitude coherent beams.

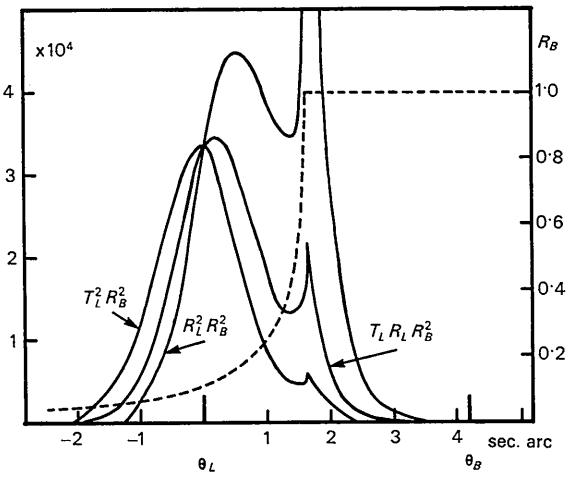

Fig. 8. The variation of the intensities of components of the exit beams in an L–B–B–L interferometer. $T_L^2 R_B^2$, $R_L^2 R_B^2$, $T_L R_L R_B^2$ for the silicon 220 reflexion of copper $K\alpha$ radiation, derived from Fig. 2.

* Supplied by Texas Instruments Inc., Dallas, Texas.

† In 1 vol. 40 % HF + 19 vol. 65 % HNO_3 with continuous agitation.

Good contrast is therefore expected and is indeed observed (Fig. 7).

Conclusions

Of the two simple types of Laue–Bragg X-ray interferometer considered, the B–L–B type seems less favourable than the L–B–L type. While the necessary geometric orientation requirements are rather stringent in the simple interferometers, they are considerably relaxed in the L–B–B–L design and satisfactory X-ray interference fringes were obtained with an interferometer of that type.

Because the Laue-angle θ_L and the Bragg-angle θ_B are not quite equal the intensity obtained with these interferometers was rather poor. With tuning, the intensities could exceed those which have been obtained with either Laue-interferometers or with Bragg-case interferometers. Herein lies an important advantage of Laue–Bragg interferometers.

This work was supported in part by the Science Research Council and by the Deutsche Forschungsgemeinschaft. One of us (M.H.) is grateful to the Deutscher Akademischer Austauschdienst for a travel grant.

References

BONSE, U. & HART, M. (1965*a*). *Appl. Phys. Let.* **6**, 155.
BONSE, U. & HART, M. (1965*b*). *Appl. Phys. Let.* **7**, 99.
BONSE, U. & HART, M. (1965*c*). *Z. Physik*, **188**, 154.
BONSE, U. & HART, M. (1966*a*). *Z. Physik*, **190**, 455.
BONSE, U. & HART, M. (1966*b*). *Z. Physik*, **194**, 1.
DARWIN, C. G. (1914). *Phil. Mag.* **27**, 315, 675.
EWALD, P. P. (1917). *Ann. Phys. Lpz.* **54**, 519.
OKKERSE, B. (1963). *Philips Res. Repts.* **18**, 413.